Eur. Phys. J. B (2012) 85: 340
DOI: 10.1140/epjb/e2012-30184-1

THE EUROPEAN PHYSICAL JOURNAL B

Regular Article

A comparison study of phase-field models for an immiscible binary mixture with surfactant

Y. Li and J. Kim[a]

Department of Mathematics, Korea University, 136-713 Seoul, Republic of Korea

Received 2 March 2012 / Received in final form 30 July 2012
Published online 10 October 2012 – © EDP Sciences, Società Italiana di Fisica, Springer-Verlag 2012

Abstract. The Ginzburg-Landau free energy functional with two order parameters has been widely used to describe surfactant adsorption phenomena at the interface between two immiscible fluids such as oil and water. To model surfactant adsorption, additional surfactant related terms are added to the original free energy functional which models an immiscible binary mixture. In this paper, we present a detailed comparison of phase-field models for an immiscible binary mixture with surfactant. In particular, we investigate the effects of mathematical model parameters on equilibrium surfactant profile across the interface between the immiscible binary mixture. Most previous models have severe time-step constraints due to the nonlinear coupling of order parameters. To solve these stability problems, we propose a special case of these models which allows the use of a much larger time-step size. We also apply a type of unconditionally gradient stable scheme and a fast multigrid method to solve the proposed model efficiently and accurately.

1 Introduction

Interfacial tension between two immiscible fluids arises from an imbalance of their respective cohesive forces at the interface and is sensitive to the presence of surfactants. Surfactants are amphophilic compounds which contain both hydrophobic and hydrophilic groups (see Fig. 1).

Surfactant molecules modify the properties of the water/oil interface. Because of these properties, surfactants have been widely used in industrial fields for various purposes. Examples are improving oil recovery [1], food processing [2,3], and forming a variety of different structures [4,5]. Recently, there has been interest in two-phase flows in microchannels [6–9].

Up to now, a number of theoretical or numerical studies have been reported to identify the mechanisms of droplet deformation [10–13], breakup and coalescence [14–16] in the presence of surfactants. In general, an immiscible binary mixture is described by the Ginzburg-Landau free energy functional, which induces the Cahn-Hilliard type equation [17] governing the time dependent behavior of fluids. To capture surfactant effects, various forms of additional functionals [18–25] such as Teramoto and Yonezawa's [22], Theissen and Gompper's [23], Sman and Graaf's [24], and Teng et al.'s [25] are proposed.

In this paper, we perform a comparison study of phase-field models for an immiscible binary mixture with surfactant and consider a special case of various models. Most previous models have severe time-step constraints due to the nonlinear coupling of order parameters. However, our proposed model allows the use of a much larger time-step size. The governing equations are solved by an efficient and accurate nonlinear multigrid method at the implicit time step.

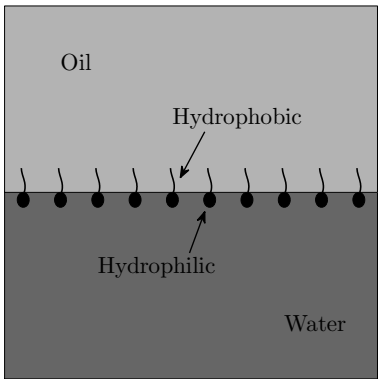

Fig. 1. Schematic illustration of the two immiscible fluids and surfactant system.

The rest of this paper is organized as follows: in Section 2, we briefly review four different phase-field models for an immiscible binary mixture with surfactant and consider a special case of these models which allows the use of a much larger time-step size. Numerical experiments such as the effects of mathematical model parameters are presented in Section 3. Finally, conclusions are given in Section 4.

[a] e-mail: cfdkim@korea.ac.kr

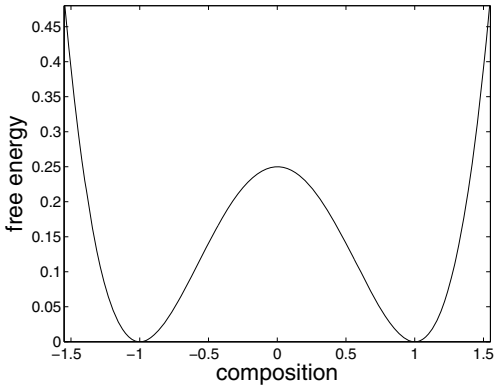

Fig. 2. A double well potential, $(\phi^2-1)^2/4$.

2 Governing equations

The thermodynamics of a fluid mixture system is determined by its free energy functional. The Ginzburg-Landau free energy functional has been commonly used to describe a binary mixture

$$\mathfrak{F}(\phi) = \int_\Omega F(\phi) d\mathbf{x},$$
$$F(\phi) = \frac{1}{4}(\phi^2-1)^2 + \frac{\epsilon_\phi}{2}|\nabla\phi|^2,$$

where an order parameter ϕ represents two immiscible fluid phases corresponding to $\phi = 1$ and $\phi = -1$. And the interface is defined by $\phi = 0$. The double-well potential $(\phi^2-1)^2/4$ is the Helmholtz free energy as shown in Figure 2. The small positive constant ϵ_ϕ is the gradient energy coefficient related to the interfacial energy and Ω is a domain.

By adding a surfactant related additional term $G(\phi,\psi)$ to $F(\phi)$, phase-field models for an immiscible binary mixture with surfactant are given as the following free energy functional:

$$\mathcal{E}(\phi,\psi) = \int_\Omega [F(\phi) + G(\phi,\psi)] d\mathbf{x}, \tag{1}$$

where ψ is the surfactant concentration. In this section, we briefly review the additional function $G(\phi,\psi)$ in four different free energy functionals such as Teramoto and Yonezawa's [22], Theissen and Gompper's [23], Sman and Graaf's [24], and Teng et al.'s [25]. Furthermore we will introduce our proposed model which is a special case of previous models.

2.1 Teramoto and Yonezawa's energy functional

In [22], Teramoto and Yonezawa proposed the two order parameter Ginzburg-Landau free energy functional with an additional term

$$G(\phi,\psi) = -\frac{s\psi}{2}|\nabla\phi|^2 + \frac{\epsilon_\psi}{2}|\nabla\psi|^2 + \frac{w}{2}(\psi-\psi_{ave})\phi^2 + \frac{\lambda}{2}(\psi-\psi_{ave})^2, \tag{2}$$

where s, ϵ_ψ, w, λ are positive phenomenological parameters and ψ_{ave} is the averaged value of ψ. In the function $G(\phi,\psi)$, the term $-0.5s\psi|\nabla\phi|^2$ prefers a relatively high value of ψ at water-oil interfaces. $0.5\epsilon_\psi|\nabla\psi|^2$ is the diffusion for surfactant. The term $0.5w(\psi-\psi_{ave})\phi^2$ favors smaller value of ψ than the average surfactant concentration. Since the total surfactant concentration should be conserved, ψ tends to have higher values around interfacial region ($\phi^2 \ll 1$) and lower values in the bulk phases ($\phi^2 \approx 1$). The term $\lambda(\psi-\psi_{ave})^2$ prevents the surfactants from forming clusters. The chemical potentials $\delta\mathcal{E}/\delta\phi$ and $\delta\mathcal{E}/\delta\psi$ are obtained via the variational derivatives of the energy functional (1) with respect to ϕ and ψ, respectively. Then, the time evolution equations of $\phi(\mathbf{x},t)$ and $\psi(\mathbf{x},t)$ are given as

$$\frac{\partial\phi}{\partial t} = M_\phi \Delta\frac{\delta\mathcal{E}}{\delta\phi}, \tag{3}$$
$$\frac{\partial\psi}{\partial t} = M_\psi \Delta\frac{\delta\mathcal{E}}{\delta\psi}, \tag{4}$$
$$\frac{\delta\mathcal{E}}{\delta\phi} = \phi^3 - \phi - \epsilon_\phi\Delta\phi + s\nabla\cdot(\psi\nabla\phi) + w(\psi-\psi_{ave})\phi, \tag{5}$$
$$\frac{\delta\mathcal{E}}{\delta\psi} = -\epsilon_\psi\Delta\psi - \frac{s}{2}|\nabla\phi|^2 + \frac{w}{2}\phi^2 + \lambda(\psi-\psi_{ave}), \tag{6}$$

where M_ϕ and M_ψ are the mobilities of ϕ and ψ, respectively.

2.2 Theissen and Gompper's energy functional

Theissen and Gompper [23] chose a slightly different form of free energy function to study the dynamics of spontaneous emulsification:

$$G(\phi,\psi) = -\frac{s\psi}{2}|\nabla\phi|^2 + \frac{\epsilon_\psi}{2}|\nabla\psi|^2 + \frac{w}{2}\psi\phi^2 + \frac{\lambda}{2}\psi^2 + \frac{v\psi}{2}(\Delta\phi)^2,$$

where v is a positive parameter and the term $v\psi(\Delta\phi)^2$ prefers relatively low values of ψ at the interface. The other terms have the similar effects as in Teramoto and Yonezawa's model, which we have described. Then $\delta\mathcal{E}/\delta\phi$ and $\delta\mathcal{E}/\delta\psi$ are given as

$$\frac{\delta\mathcal{E}}{\delta\phi} = \phi^3 - \phi - \epsilon_\phi\Delta\phi + s\nabla\cdot(\psi\nabla\phi) + w\psi\phi + v\Delta(\psi\Delta\phi), \tag{7}$$
$$\frac{\delta\mathcal{E}}{\delta\psi} = -\epsilon_\psi\Delta\psi - \frac{s}{2}|\nabla\phi|^2 + \frac{w}{2}\phi^2 + \lambda\psi + \frac{v}{2}(\Delta\phi)^2. \tag{8}$$

2.3 Sman and Graaf's energy functional

In [24], Sman and Graaf proposed the following energy function

$$G(\phi,\psi) = -\frac{s\psi}{2}|\nabla\phi|^2 + \frac{w}{2}\psi\phi^2 + \lambda\left[\psi\ln\psi + (1-\psi)\ln(1-\psi)\right]. \tag{9}$$

Here $\lambda[\psi\ln\psi+(1-\psi)\ln(1-\psi)]$ is the entropy term and restricts the value of ψ to be in the range $[0,1]$ and models the surfactant system by inducing a Fickian type equation [26] for ψ in fluids. Then we have

$$\frac{\delta\mathcal{E}}{\delta\phi}=\phi^3-\phi-\epsilon_\phi\Delta\phi+s\nabla\cdot(\psi\nabla\phi)+w\phi\psi, \tag{10}$$

$$\frac{\delta\mathcal{E}}{\delta\psi}=-\frac{s}{2}|\nabla\phi|^2+\frac{w}{2}\phi^2+\lambda[\ln\psi-\ln(1-\psi)]. \tag{11}$$

2.4 Teng et al.'s energy functional

In [25], Teng et al. set the additional energy term as follows:

$$G(\phi,\psi)=\frac{s}{2}(\psi-|\nabla\phi|)^2+\lambda\left[\psi\ln\psi+(1-\psi)\ln(1-\psi)\right].$$

The first term $0.5s(\psi-|\nabla\phi|)^2$ makes the surfactant concentration profile be similar to the fluid interface profile. Then we have

$$\frac{\delta\mathcal{E}}{\delta\phi}=\phi^3-\phi-(\epsilon_\phi+s)\Delta\phi+s\nabla\cdot\left(\psi\frac{\nabla\phi}{|\nabla\phi|}\right), \tag{12}$$

$$\frac{\delta\mathcal{E}}{\delta\psi}=s(\psi-|\nabla\phi|)+\lambda[\ln\psi-\ln(1-\psi)]. \tag{13}$$

2.5 Proposed energy functional

As a special case from previous models, we propose a simple and numerically robust model. The term $-s\psi|\nabla\phi|^2$ favors the surfactants to sit at water-oil interfaces and $\epsilon_\psi|\nabla\psi|^2$ is the diffusion for surfactant. Thus depending on the magnitude of parameters s and ϵ_ψ in the two functions, surfactants can sharply or smoothly accumulate in the interface. To prevent surfactants from forming clusters, we consider the term $\psi\ln\psi+(1-\psi)\ln(1-\psi)$. For the stability of numerical computation, we replace $\psi\ln\psi+(1-\psi)\ln(1-\psi)$ by $-4\ln(2)\psi(1-\psi)$ (see Fig. 3). Finally, we propose the following additional energy function

$$G(\phi,\psi)=-\frac{s\psi}{2}|\nabla\phi|^2+\frac{\epsilon_\psi}{2}|\nabla\psi|^2-\lambda\psi(1-\psi). \tag{14}$$

Then we have the following chemical potentials of ϕ and ψ:

$$\frac{\delta\mathcal{E}}{\delta\phi}=\phi^3-\phi-\epsilon_\phi\Delta\phi+s\nabla\cdot(\psi\nabla\phi), \tag{15}$$

$$\frac{\delta\mathcal{E}}{\delta\psi}=-\frac{s}{2}|\nabla\phi|^2-\epsilon_\psi\Delta\psi+\lambda(2\psi-1). \tag{16}$$

For simplicity, the boundary conditions are imposed as the zero Neumann boundary conditions on the domain Ω:

$$\mathbf{n}\cdot\nabla\phi=\mathbf{n}\cdot\nabla\psi=\mathbf{n}\cdot\nabla\frac{\delta\mathcal{E}}{\delta\phi}=\mathbf{n}\cdot\nabla\frac{\delta\mathcal{E}}{\delta\psi}=0, \tag{17}$$

where $\mathbf{n}$ is a unit normal vector to $\partial\Omega$.

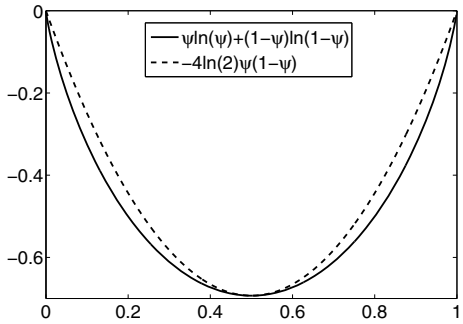

Fig. 3. Plots of $\psi\ln\psi+(1-\psi)\ln(1-\psi)$ and $-4\ln(2)\psi(1-\psi)$.

Table 1. Parameter values for five models. Here × means that the corresponding term is not used.

Parameter	s	ϵ_ψ	w	λ	v
Teramoto and Yonezawa	0.5	0.5	0.1	0.1	×
Theissen and Gompper	0.25	0.4	0.1	0.1	0.05
Sman and Graaf	0.1	×	0.1	0.02	×
Teng et al.	0.1	×	×	0.01	×
Proposed	0.48	0.4	×	0.05	×

3 Numerical experiments

Numerical solution is described in Appendix. In numerical experiments, we consider that numerical solutions are at steady state when the difference between the consecutive solutions ψ^{n+1} and ψ^n becomes less than a given tolerance, $tol=10^{-6}$. We perform numerical experiments on the computational domain $\Omega=(0,128)$ with a 512 grid. Initial conditions for $\phi(x)$ and $\psi(x)$ are

$$\phi(x)=\tanh\left((x-64)/(\sqrt{2\epsilon_\phi})\right)\ \text{ and }\ \psi(x)=0.1.$$

And we take parameters as $M_\phi=M_\psi=1$, $\Delta t=0.01$, and $\epsilon_\phi=1.442$.

3.1 Effects of parameters

In this section we will test the effect of parameters from the five phase-field models. Unless otherwise specified, we use the following parameters which are summarized in Table 1. The steady surfactant shapes are shown in Figure 4.

3.1.1 Teramoto and Yonezawa's energy functional

In this subsection, we present several numerical experiments to show the effect of each term in the Teramoto and Yonezawa's energy functional with various ϵ_ψ, s, w, and λ values.

In Figure 5a, three different values of $s=0.75, 0.5, 0.25$ are used for comparison. The grey region represents the transition layer of phase-field, i.e., $\phi\in(-0.95,0.95)$. We observe that larger s makes more surfactants gather at the interface between two immiscible fluids as expected from the term $-0.5s\psi|\nabla\phi|^2$. We use three different values of $\epsilon_\psi=1,\ 0.5,\ 0.25$ in Figure 5b. From the results, we

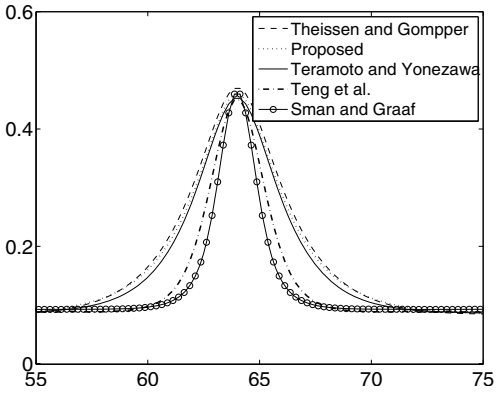

Fig. 4. Plots for numerical results with the parameters in Table 1.

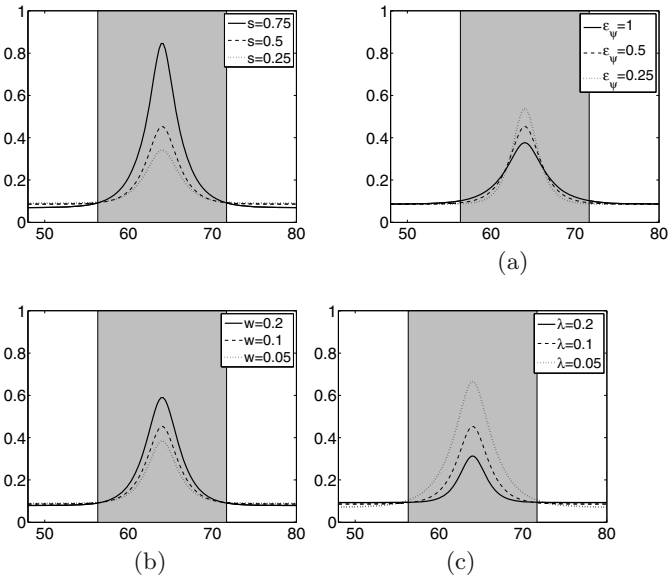

Fig. 5. (a), (b), (c), and (d) show the effect of s, ϵ_ψ, w, and λ in Teramoto and Yonezawa's model, respectively.

can observe that when the parameter ϵ_ψ decreases, the interface of surfactants becomes sharper due to the diffusion term $0.5\epsilon_\psi|\nabla\psi|^2$. The coupling term $0.5w(\psi-\psi_{ave})\phi^2$ guarantees small local surfactant concentration in the bulk phases [24]. Figure 5c shows the effect of this local coupling term with three different values of $w = 0.2,\ 0.1$, and 0.05. For parameter λ, as we can see from Figure 5d, larger λ causes the interface of surfactants smooth as we expect from the term $0.5\lambda(\psi-\psi_{ave})^2$. Here three different values $\lambda = 0.2,\ 0.1,\ 0.05$ are used.

3.1.2 Theissen and Gompper's energy functional

In Figures 6a–6e, we show the effect of model parameters ϵ_ψ, s, w, λ, and v. ϵ_ψ, s, w, and λ have similar effects as Teramoto and Yonezawa's energy functional. In Figure 6a, three different values of $s = 0.5,\ 0.25,\ 0.1$ are used to show the effect of $-0.5s\psi|\nabla\phi|^2$. To show the effect of the term $0.5\epsilon_\psi|\nabla\psi|^2$, we use parameters $\epsilon_\psi = 1,\ 0.4,\ 0.1$

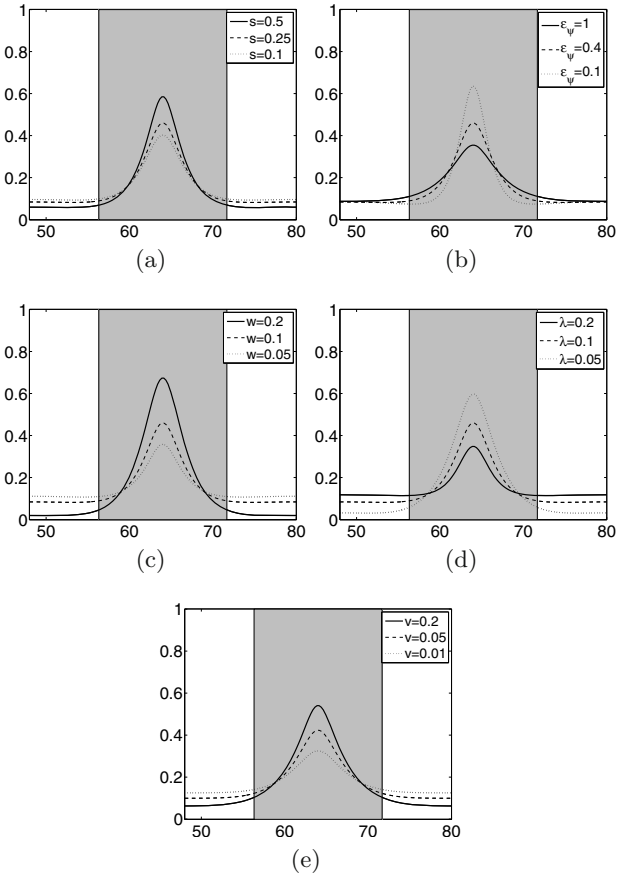

Fig. 6. (a), (b), (c), (d), and (e) show the effect of s, ϵ_ψ, w, λ, and v in Theissen and Gompper's model, respectively.

in Figure 6b. Figure 6c shows the effect of $0.5w\psi\phi^2$ by using three different values of $w = 0.2,\ 0.1,\ 0.05$. Figure 6d shows the effect of the term $0.5\lambda\psi^2$. Here three different values of $\lambda = 0.2,\ 0.1,\ 0.05$ are used. Figure 6e shows the effect of this term with three different values $v = 0.2,\ 0.05,\ 0.01$.

3.1.3 Sman and Graaf's energy functional

In Figure 7, we show the effect of additional term by the parameters s, w, and λ. The term $0.5s\psi|\nabla\phi|^2$ means the nonlocal coupling term and plays a role to perform the preference of surfactant at the phase-field interface. From the results shown in Figure 7a, we observe that larger s makes interfacial profile sharper. Here three different values of $s = 0.2,\ 0.1,\ 0.05$ are used. In Figure 7b, we use three different values of $w = 0.15,\ 0.1,\ 0.05$. As can be seen that the larger w also causes ψ to grow faster, since this term is introduced to gather the surfactant at the interface. In numerical experiment for λ shown in Figure 7c, the smaller λ also causes ψ to grow sharper. Here three different values of $\lambda = 0.04,\ 0.02,\ 0.01$ are used.

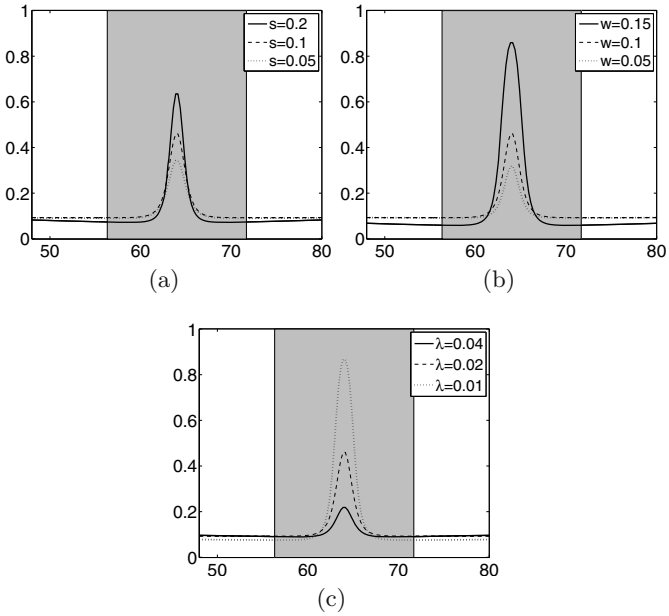

Fig. 7. (a), (b), and (c) show the effect of s, w, and λ in Sman and Graaf's model, respectively.

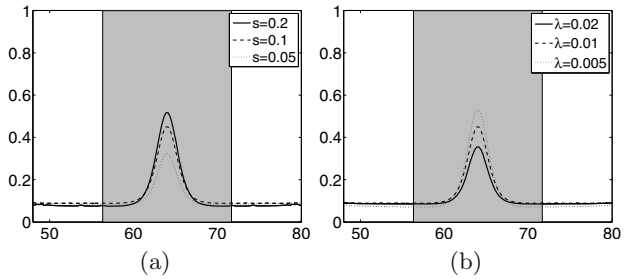

Fig. 8. (a) and (b) show the effect of s and λ in Teng et al.'s model, respectively.

3.1.4 Teng et al.'s energy functional

Teng et al. introduce the additional term $s(\psi - |\nabla\phi|)^2$, which makes surfactants move to the interfaces until $\psi \sim |\nabla\phi|$ [25,27]. Thus as times goes on, the surfactant concentration diffuses to the bulk region and accumulates at the interfacial region. In Figure 8a, we use three different values of $s = 0.2,\ 0.1$, and 0.05. It can be observed that the larger s is used, the more surfactants are gathered at the interface. These results also suggest that ψ indeed approaches $|\nabla\phi|$. And the numerical result for $\lambda\left[\psi\ln\psi + (1-\psi)\ln(1-\psi)\right]$ term is shown in Figure 8b with three different values of $\lambda = 0.02,\ 0.01$, and 0.005.

3.1.5 Proposed energy functional

Since we already studied the effect of the terms $-0.5s\psi|\nabla\phi|^2$ and $0.5\epsilon_\psi|\nabla\psi|^2$, we focus on the term $-\lambda\psi(1-\psi)$, which is a replacing term for $\lambda[\psi\ln\psi + (1-\psi)\ln(1-\psi)]$. To show the numerical stability of our model, we consider a numerical test with two models. One is our proposed model and the other is with $\lambda[\psi\ln\psi + (1-\psi)\ln(1-\psi)]$. The parameters are chosen as $s = 0.2$ and $\epsilon_\psi = 0.2$. To match two terms, $-0.015\psi(1-\psi)$ and $0.005[\psi\ln\psi + (1-\psi)\ln(1-\psi)]$ are used. Figure 9a shows the result with a small time step $\Delta t = 1$. Both models generate similar results. Figure 9b shows the result with a large time step $\Delta t = 100$. The result suggests that with a large time step the model with the term $\psi\ln\psi + (1-\psi)\ln(1-\psi)$ shows oscillations.

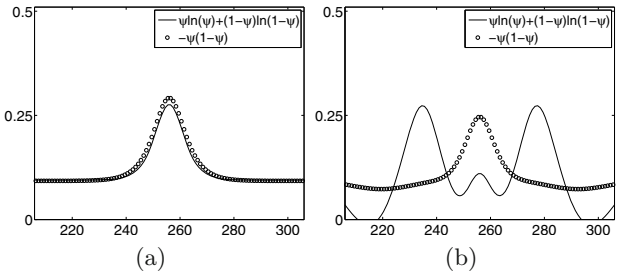

Fig. 9. (a) and (b) are results with $\Delta t = 1$ and $\Delta t = 100$.

3.2 The positiveness of surfactant concentration

Theoretically, the order parameter ψ for the surfactant is in the range $[0, 1]$. However, numerical solutions may suffer nonphysical ψ such as negative values during calculations. In this section, we present several numerical examples which show negative values of surfacants ψ for each model.

3.2.1 Teramoto and Yonezawa's energy functional

Figure 10 shows that ψ may be negative with unsuitable parameters s, w, and λ. In Figure 10a, we use $\epsilon_\psi = 1$, $s = 2.5$, $w = 0.1$, and $\lambda = 0.1$. It can be observed that ψ at time $t = 5$ becomes negative. To show a nonphysical phenomenon due to w, we use $\epsilon_\psi = 1$, $s = 0.5$, $w = 0.4$, and $\lambda = 0.1$ in Figure 10b. Figure 10c shows a nonphysical phenomenon due to small λ value. Here $\epsilon_\psi = 1$, $s = 0.5$, $w = 0.1$, and $\lambda = 0.02$ are used. Note that although there are nonphysical phenomena due to the unsuitable parameters, the Teramoto and Yonezawa's model is stable.

3.2.2 Theissen and Gompper's energy functional

In Figure 11a, we use $\epsilon_\psi = 1$, $s = 1$, $w = 0.1$, $\lambda = 0.1$, and $v = 0.1$. $\epsilon_\psi = 1$, $s = 0.5$, $w = 0.25$, $\lambda = 0.01$, and $v = 0.1$ in Figure 11b. $\epsilon_\psi = 1$, $s = 0.5$, $w = 0.1$, $\lambda = 0.03$, and $v = 0.1$ are used in Figure 11c. As we can see from Figure 11, negative values of ϕ are observed. However, these simulations are stable without oscillations.

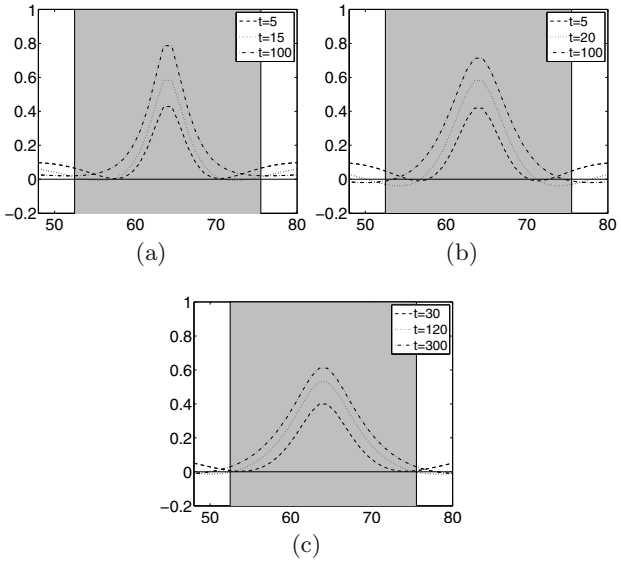

Fig. 10. The time evolution of ψ with unsuitable value of parameters in Teramoto and Yonezawa's model. (a) $s = 2.5$, (b) $w = 0.4$, and (c) $\lambda = 0.02$.

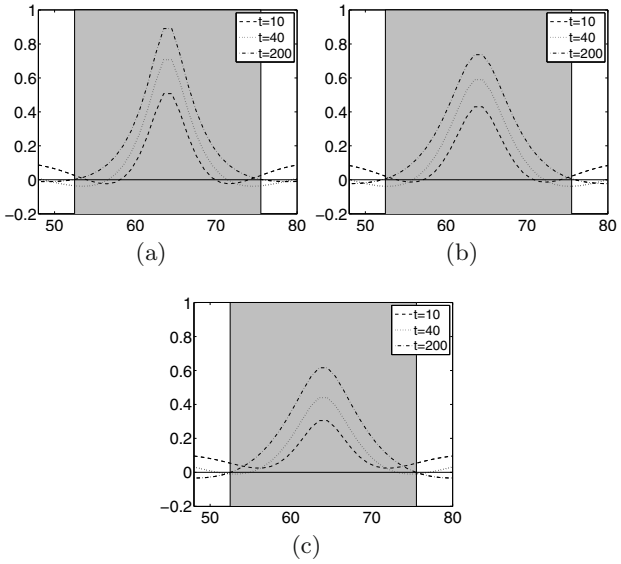

Fig. 11. The time evolution of ψ with unsuitable value of (a) s, (b) w, and (c) λ in Theissen and Gompper's model, respectively. Computational parameters: (a) $\epsilon_\psi = 1$, $s = 1$, $w = 0.1$, $\lambda = 0.1$, and $v = 0.1$. (b) $\epsilon_\psi = 1$, $s = 0.5$, $w = 0.25$, $\lambda = 0.01$, and $v = 0.1$. (c) $\epsilon_\psi = 1$, $s = 0.5$, $w = 0.1$, $\lambda = 0.03$, and $v = 0.1$.

3.2.3 Sman and Graaf's energy functional

For Sman and Graaf's energy functional, due to the term $\lambda[\ln\psi - \ln(1-\psi)]$, oscillations occurred at the zero value of ψ as shown in Figures 12a–12c. To observe this, we use $s = 0.5$, $w = 0.1$, $\lambda = 0.02$, and $s = 0.1$, $w = 0.5$, $\lambda = 0.02$ in Figures 12a and 12b, respectively. And $s = 0.1$, $w = 0.1$, and $\lambda = 0.008$ are used in Figure 12c. In Figure 12, oscillations are observed.

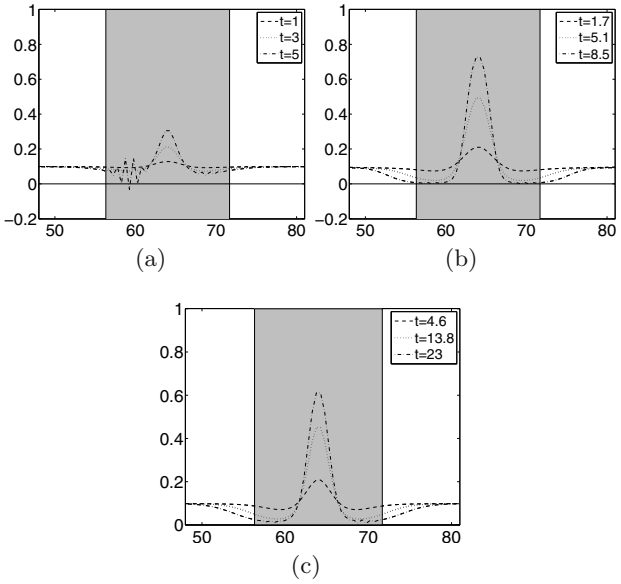

Fig. 12. The time evolution of ψ with unsuitable values of (a) $s = 0.5$, (b) $w = 0.5$, and (c) $\lambda = 0.008$ in Sman and Graaf's model, respectively.

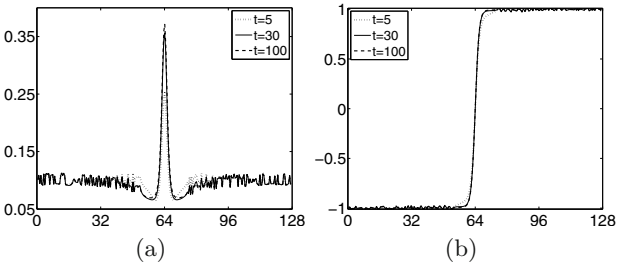

Fig. 13. The time evolution of (a) ψ and (b) ϕ in Teng et al.'s model.

3.2.4 Teng et al.'s energy functional

Let us consider the term $0.5s(\psi - |\nabla\phi|)^2$ in Teng et al.'s energy functional. The profile of ψ resembles that of ϕ. Therefore ϕ cannot be stable when ψ is unstable. To confirm that, we set numerical experiments with $s = 1$ and $\lambda = 0.1$. Figure 13 shows nonphysical phenomena. Since $\psi \sim |\nabla\phi|$, if the oscillation for surfactant concentration occurs, the water-oil interface also occurs.

3.2.5 Proposed energy functional

The term $-0.5s\psi|\nabla\phi|^2$ is used to model the high value of ψ at the interface of water and oil. Thus if we use a large value of s, surfactants quickly absorb to the interface so that ψ may be negative as shown in Figure 14a. Here, we use $s = 0.5$, $\epsilon_\phi = 0.02$, and $\lambda = 0.02$. Also, as we mentioned above, we proposed the term $-\lambda\psi(1-\psi)$ to restrict the value of ψ in the range $[0, 1]$. It is possible that with a small λ value, ψ may be negative. To see this, we show the evolution of ψ in Figure 14b with $s = 0.25$,

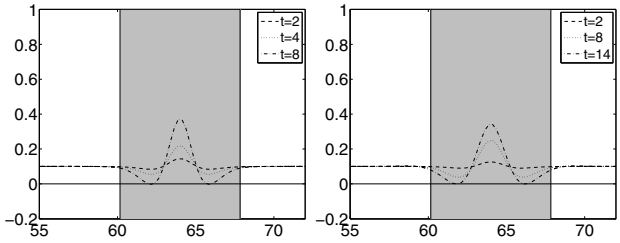

Fig. 14. The time evolution of ψ with unsuitable values of (a) $s = 0.5$ and (b) $\lambda = 0.01$ in our proposed model, respectively.

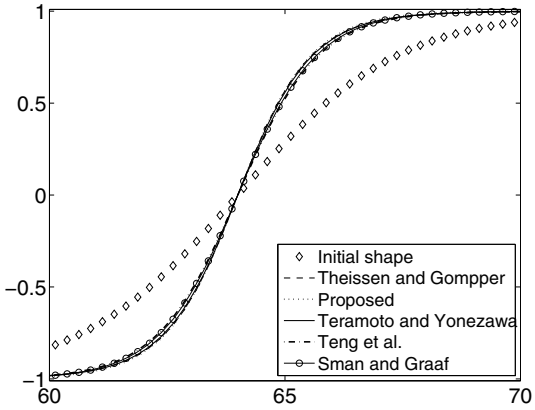

Fig. 15. Plots for phase-field ϕ profiles.

$\epsilon_\phi = 0.02$, and $\lambda = 0.01$. However, the solution is stable and does not have oscillations.

4 Conclusions

In this paper, we presented a detailed comparison of phase-field models such as Teramoto and Yonezawa's, Theissen and Gompper's, Sman and Graaf's, and Teng et al.'s for a surfactant adsorption phenomena at the interface between two immiscible fluids. Most previous models had severe time-step constraints due to the nonlinear coupling of order parameters. To solve these stability problems, we proposed a special case of these models which allows the use of a much large time-step size. We also applied a type of unconditionally gradient stable scheme and a fast multigrid method to solve the proposed model efficiently and accurately.

From the numerical calculation in Figure 4, we drew an important physical modeling of surfactant systems. Since there are coupling terms in the free energy functional from all models, the equilibrium profiles of the phase-field ϕ are modified with presence of surfactant. Figure 15 shows the equilibrium profiles of ϕ. Here we used same parameters in Figure 4. All models generated similar results showing steeper gradient of phase-field profiles across interface region. In general, surfactant lows the interfacial tension. However, this result indicates that surfactant presence actually increases surface energy by making sharp interface transitions. As future research, we investigate the effect of this side effect on surface tension modeling with hydrodynamics.

This research was supported by Basic Science Research Program through the National Research Foundation of Korea (NRF) funded by the Ministry of Education, Science and Technology (No. 2011-0023794). The authors thank the reviewers for the constructive and helpful comments on the revision of this article.

Appendix: Numerical solution

We shall discretize the two immiscible fluids and surfactant system in one-dimensional space, i.e., $\Omega = (a, b)$. Let N be a positive even integer, $h = (b-a)/N$ be a uniform grid size, and $\Omega_h = \{x_i = (i-0.5)h,\ 1 \le i \le N\}$ be the set of cell-centers. Let us denote the numerical approximation of the solutions by $(\phi_i^n, \psi_i^n) = (\phi(x_i, n\Delta t), \psi(x_i, n\Delta t))$, where $i = 1, \ldots, N$ and $n = 0, 1, \ldots, N_t$. Here, $\Delta t = T/N_t$ is the time step, T is the final time, and N_t is the total number of time steps. The zero Neumann boundary condition equation (17) is applied for each n as

$$\nabla_h \phi^n_{\frac{1}{2}} = \nabla_h \left(\frac{\delta \mathcal{E}}{\delta \phi}\right)^n_{\frac{1}{2}} = \nabla_h \psi^n_{\frac{1}{2}} = \nabla_h \left(\frac{\delta \mathcal{E}}{\delta \psi}\right)^n_{\frac{1}{2}} = 0,$$
$$\nabla_h \phi^n_{N+\frac{1}{2}} = \nabla_h \left(\frac{\delta \mathcal{E}}{\delta \phi}\right)^n_{N+\frac{1}{2}} = 0,$$
$$\nabla_h \psi^n_{N+\frac{1}{2}} = \nabla_h \left(\frac{\delta \mathcal{E}}{\delta \psi}\right)^n_{N+\frac{1}{2}} = 0.$$

Here the discrete differential operator is $\nabla_h \phi^n_{i+\frac{1}{2}} = (\phi^n_{i+1} - \phi^n_i)/h$ and the other terms are similarly defined. Let the discrete Laplacian operator be defined as $\Delta_h \phi_i = (\nabla_h \phi_{i+\frac{1}{2}} - \nabla_h \phi_{i-\frac{1}{2}})/h$. Then we consider a fully discrete semi-implicit finite difference scheme for the models, which we have introduced in Section 2.

A.1 Teramoto and Yonezawa' energy functional

We discretize equations (3)–(6) as

$$\frac{\phi^{n+1} - \phi^n}{\Delta t} = M_\phi \Delta_h \nu^{n+1} - M_\phi \Delta_h \phi^n, \tag{A.1}$$
$$\nu^{n+1} = (\phi^{n+1})^3 - \epsilon_\phi \Delta_h \phi^{n+1} + s \nabla_h \cdot (\psi^n \nabla_h \phi^n) + w(\psi^n - \psi_{ave})\phi^n, \tag{A.2}$$
$$\frac{\psi^{n+1} - \psi^n}{\Delta t} = M_\psi \Delta_h \mu^{n+1}, \tag{A.3}$$
$$\mu^{n+1} = -\epsilon_\psi \Delta_h \psi^{n+1} - \frac{s}{2} \left|\nabla_h \phi^{n+1}\right|^2 + \frac{w}{2}(\phi^{n+1})^2 + \lambda(\psi^{n+1} - \psi_{ave}). \tag{A.4}$$

A.2 Theissen and Gompper's energy functional

Equations (7) and (8) are discretized as

$$\begin{aligned}\nu^{n+1} &= (\phi^{n+1})^3 - \epsilon_\phi \Delta_h \phi^{n+1} + s\nabla_h \cdot (\psi^n \nabla_h \phi^n) \\ &\quad + w\psi^n \phi^n + v\Delta_h(\psi^n \Delta_h \phi^n), \\ \mu^{n+1} &= -\epsilon_\psi \Delta_h \psi^{n+1} - \frac{s}{2}\left|\nabla_h \phi^{n+1}\right|^2 + \frac{w}{2}(\phi^{n+1})^2 \\ &\quad + \lambda\psi^{n+1} + \frac{v}{2}(\Delta_h \phi^{n+1})^2.\end{aligned}$$

A.3 Sman and Graaf's energy functional

We discretize equations (10) and (11) as

$$\begin{aligned}\nu^{n+1} &= (\phi^{n+1})^3 - \epsilon_\phi \Delta_h \phi^{n+1} + s\nabla_h \cdot (\psi^n \nabla_h \phi^n) \\ &\quad + w\psi^n \phi^n, \\ \mu^{n+1} &= -\frac{s}{2}\left|\nabla_h \phi^{n+1}\right|^2 + \frac{w}{2}(\phi^{n+1})^2 \\ &\quad + \lambda\left(\ln(\psi^n) - \ln(1-\psi^n)\right).\end{aligned}$$

A.4 Teng et al.'s energy functional

Equations (12) and (13) are discretized as

$$\begin{aligned}\nu^{n+1} &= (\phi^{n+1})^3 - (\epsilon_\phi + s)\Delta_h \phi^{n+1} + s\nabla_h \cdot \left(\psi^n \frac{\nabla_h \phi^n}{|\nabla_h \phi^n|}\right), \\ \mu^{n+1} &= s(\psi^{n+1} - |\nabla_h \phi^{n+1}|) + \lambda\left(\ln(\psi^n) - \ln(1-\psi^n)\right).\end{aligned}$$

Here we add a small value $\delta = 10^{-6}$ in the denominator to avoid singularities and then get the following term

$$\begin{aligned}\nabla_h \cdot \left(\psi^n \frac{\nabla_h \phi^n}{|\nabla_h \phi^n|}\right) &= \frac{(\psi^n_{i+1} + \psi^n_i)}{2h} \frac{\phi^n_{i+1} - \phi^n_i}{|\phi^n_{i+1} - \phi^n_i| + \delta} \\ &\quad - \frac{(\psi^n_i + \psi^n_{i-1})}{2h} \frac{\phi^n_i - \phi^n_{i-1}}{|\phi^n_i - \phi^n_{i-1}| + \delta}.\end{aligned}$$

A.5 Proposed energy functional

We discretize equations (15) and (16) as

$$\nu^{n+1} = (\phi^{n+1})^3 - \epsilon_\phi \Delta_h \phi^{n+1} + s\nabla_h \cdot (\psi^n \nabla_h \phi^n), \quad \text{(A.5)}$$

$$\mu^{n+1} = -\frac{s}{2}|\nabla_h \phi^{n+1}|^2 - \epsilon_\psi \Delta_h \psi^{n+1} + \lambda(2\psi^n - 1). \quad \text{(A.6)}$$

A.6 Numerical solution-nonlinear multigrid solver

In this section, we use a nonlinear full approximation storage (FAS) multigrid method to solve the nonlinear discrete system (Eqs. (A.1), (A.3), (A.5), and (A.6)) at the implicit time level. The basic idea of the multigrid method is to accelerate the solution of a fine grid problem by computing corrections on a coarse grid and then interpolating them back to the fine grid problem. At each grid level, the discrete equations are solved by a pointwise Gauss–Seidel relaxation scheme. Here we only describe the relaxation with our proposed method and for additional details, please refer to [28]. The algorithm of the nonlinear multigrid method for solving the discrete system begins with rewriting equations (A.1) and (A.5) as follows.

$$N(\phi^{n+1}, \nu^{n+1}) = (\varphi^n, \upsilon^n),$$

where $N(\phi^{n+1}, \nu^{n+1}) = (\phi^{n+1}/\Delta t - M_\phi \Delta_h \nu^{n+1}, \nu^{n+1} - (\phi^{n+1})^3 + \epsilon_\phi \Delta_h \phi^{n+1})$ and the source term is $(\varphi^n,\ \psi^n) = (\phi^n/\Delta t - M_\phi \Delta_h \phi^n,\ s\nabla_h \cdot (\psi^n \nabla_h \phi^n))$.

• *Relaxation*: rewriting equations (A.1) and (A.5), we get

$$\begin{aligned}&\frac{\phi^{n+1}_i}{\Delta t} + \frac{2\nu^{n+1}_i}{h^2} = \varphi^n_i + \frac{\nu^{n+1}_{i+1} + \nu^{n+1}_{i-1}}{h^2}, \\ &-\frac{2\epsilon_\phi}{h^2}\phi^{n+1}_i - (\phi^{n+1}_i)^3 + \nu^{n+1}_i = \upsilon^n_i - \frac{\epsilon_\phi}{h^2}(\phi^{n+1}_{i+1} + \phi^{n+1}_{i-1}).\end{aligned}$$

Next, we replace ϕ^{n+1}_k and ν^{n+1}_k in the above equations with $\bar\phi^m_k$ and $\bar\nu^m_k$ if $k \le i$, otherwise with ϕ^m_k and ν^m_k, i.e.,

$$\begin{aligned}&\frac{\bar\phi^m_i}{\Delta t} + \frac{2\bar\nu^m_i}{h^2} = \varphi^n_i + \frac{\nu^m_{i+1} + \bar\nu^m_{i-1}}{h^2}, \\ &-\frac{2\epsilon_\phi}{h^2}\bar\phi^m_i - (\bar\phi^m_i)^3 + \bar\nu^m_i = \upsilon^n_i - \frac{\epsilon_\phi}{h^2}(\phi^m_{i+1} + \bar\phi^m_{i-1}). \quad \text{(A.7)}\end{aligned}$$

Since $(\bar\phi^m_i)^3$ in equation (A.7) is nonlinear with respect to $\bar\phi^m_i$, we linearize $(\bar\phi^m_i)^3$ at ϕ^m_i, i.e.,

$$(\bar\phi^m_i)^3 = (\phi^m_i)^3 + 3(\phi^m_i)^2(\bar\phi^m_i - \phi^m_i).$$

After substituting this expression into equation (A.7), we obtain

$$\begin{aligned}&-\left(\frac{2\epsilon_\phi}{h^2} + 3(\phi^m_i)^2\right)\bar\phi^m_i + \bar\nu^m_i = \\ &\qquad \upsilon^n_i - \frac{\epsilon_\phi}{h^2}(\phi^m_{i+1} + \bar\phi^m_{i-1}) - 2(\phi^m_i)^2.\end{aligned}$$

This completes the description of relaxation. Once the updated order parameters ϕ^{n+1} have been determined, we can find ψ^{n+1} from equations (A.3) and (A.6) using the multigrid method in a similar manner.

References

1. E.A. Spinler, D.R. Zornes, D.P. Tobola, A. Moradi-Araghi, *Phillips Petroleum Co, Improved Oil Recovery Symposium* (Tulsa, Oklahoma, 2000), pp. 3–5
2. D. Myers, *Surfactant Science and Technology*, 3rd edn. (John Wiley & Sons, Inc., Hoboken, New Jersey, 2006)
3. J. Sjöblom, *Emulsions and Emulsion Stability* (Taylor & Francis, 2006)
4. D.R. Nelson, T. Piran, S. Weinberg, *Statisrical Mechanics of Membranes and Surfaces* (World Scientific, Singapore, 1989)
5. R. Lipowsky, Nature **349**, 475 (1991)

6. R. Dreyfus, P. Tabeling, H. Willaime, Phys. Rev. Lett. **14**, 144505 (2003)
7. H. Stone, A. Stroock, A. Ajdari, Annu. Rev. Fluid Mech. **36**, 381 (2004)
8. S. van der Graaf, M.L.J. Steegmans, R.G.M. van der Sman, C.G.P.H. Schroen, R.M. Boom, Colloids Surf. **266**, 106 (2005)
9. A. Warmerdam, K.G.P.H. Schroen, R.M. Boom, Langmuir **25**, 9751 (2009)
10. I. Bazhlekov, P.D. Anderson, H.E.H. Meijer, J. Colloid Interf. Sci. **298**, 369 (2006)
11. J.J.M. Janssen, A. Boon, W.G.M. Agterof, AIChE J. **43**, 1436 (1997)
12. L.G. Leal, Phys. Fluids. **16**, 1833 (2004)
13. H. Liu, Y. Zhang, J. Comput. Phys. **229**, 9166 (2010)
14. H.A. Stone, L.G. Leal, J. Fluid Mech. **220**, 161 (1990)
15. U. Sundararaj, C.W. Macosko, Macromolecules **28**, 2647 (1995)
16. S. Tasoglu, U. Demirci, M. Muradoglu, Phys. Fluids **20**, 040805 (2008)
17. J.W. Cahn, J.E. Hilliard, J. Chem. Phys. **28**, 258 (1958)
18. G. Gompper, D. Richter, R. Strey, J. Phys.: Condens. Matter **13**, 9055 (2001)
19. G. Gompper, M. Schick, Phys. Rev. E **49**, 1478 (1994)
20. G. Gompper, S. Zschocke, Phys. Rev. A **46**, 4836 (1992)
21. G. Gompper, S. Zschocke, Europhys. Lett. **16**, 731 (1991)
22. T. Teramoto, F. Yonezawa, J. Colloid Interf. Sci. **235**, 329 (2001)
23. O. Theissen, G. Gompper, Eur. Phys. J. B **11**, 91 (1999)
24. R.G.M. Van der Sman, S. Van der Graaf, Rheol. Acta **46**, 11 (2006)
25. C.-H. Teng, I.-L. Chern, M.-C. Lai, Discrete Continuous Dyn. B **4**, 17 (2012)
26. E.B. Naumann, D.Q. He, Chem. Eng. Sci. **56**, 1999 (2001)
27. I. Fonseca, M. Morini, V. Slastikov, Arch. Ration. Mech. Anal. **183**, 411 (2007)
28. J. Kim, H.-O. Bae, J. Korean Phys. Soc. **53**, 672 (2008)